Nanoscale

PAPER

View Article Online
View Journal

Cite this: DOI: 10.1039/d6nr00232c

Silver exchange dynamics in monolayer-protected doped gold clusters

Jesse R. R. Delmage, Jeffrey T. Paci and Irina Paci *

The mechanism of inter-cluster exchange reactions remains an open problem in nanoparticle chemistry. Such reactions, first reported in 2015, involve the exchange of metal atoms between ligand-protected nanoparticles in solution and have enabled the synthesis of heterometallic clusters with precise dopant counts. While previous computational studies have proposed plausible exchange pathways, none have explicitly captured the dynamics of a cluster–cluster collision. Here, we use a direct dynamics approach combined with quantum-based semiempirical potentials to simulate collisions between silver-doped and undoped gold nanoparticles and to follow atom exchange events in real time. The simulations reveal that restructuring at the core–monolayer interface is a key initiating step, enabling exposure of core metal atoms. Subsequent transfer of silver between clusters is mediated by thiolate ligands, which stabilize the migrating atom through successive metal–sulfur interactions across the inter-cluster region. Beyond elucidating the exchange mechanism, this work demonstrates a general strategy for modeling reactive collisions and large-scale dynamical processes in nanomaterials.

Received 17th January 2026,
Accepted 11th April 2026

DOI: 10.1039/d6nr00232c

rsc.li/nanoscale

1 Introduction

Thiolate-protected gold nanoparticles (AuNPs) represent an important class of nanomaterials with applications in fields ranging from electro-catalysis to spectroscopy and even biomedicine.[1–4] Among these AuNPs, monolayer-protected clusters consist of a metallic core of small, constant size, surrounded by a self-assembled monolayer that stabilizes the cluster and controls its size. Thiolate protected AuNPs have a gold core surrounded by $SR(AuSR)_x$ (x = 1, 2) staple motifs,[3,5,6] where the residue R is normally based on an alkyl or aromatic backbone. These well-studied clusters often exist in "magic number" sizes, which are more stable relative to similar-sized, non-"magic number" clusters. Clusters included in this class are: $Au_{25}(SR)_{18}$, $Au_{38}(SR)_{24}$ and $Au_{144}(SR)_{60}$ among many others.[7–9]

The nanometer scale of AuNPs results in size-dependent quantum effects that find use in tunable materials for a variety of applications,[10–12] including drug delivery, optical coatings, and catalysis.[13–16] Besides their size, the useful properties of these clusters are further tunable by alloying with a variety of metals. Doping these nanoparticles modifies their electronic properties, helping augment their catalytic performance, enhancing quantum yield or increasing stability in solution.[17–20] Two prominent approaches exist for synthesizing alloyed AuNPs: a ground-up approach using two different metallic salts,[19,21,22] and post synthesis exchange reactions.[23,24] The latter involves reactions that occur in solution between two unique nanoparticles that lead to the formation of a bimetallic cluster. Negishi *et al.* published an example of the former method when they synthesized nanoparticles based on the "magic" Au_{38} cluster[19] from Na_2PdCl_4 and $HAuCl_2$ salts, forming $Pd_2Au_{36}(SR_{24})$. Burgi *et al.*[25] demonstrated formation of $Au_{38-x}Ag_x(SC_2H_4Ph)_{24}$ by cluster collisions in solution. The synthesis of Cu_xPdAu_{24-x} by Muller *et al.*[26] and Hossain *et al.*[27] is another example of post synthesis modification based on mixing $PdAu_{24}$ with small copper-ligand species.

A consensus on the mechanism by which metallic atoms exchange between doped and undoped AuNPs during inter-cluster reactions has not been reached. Initial works suggested that ligand–metal species could break free of one nanoparticle, diffuse in solution and bind to another AuNP.[28] Moreover, ligand–single metal atom species were observed in electrospray ionization mass spectrometry (ESI-MS) studies of Au_{25} AuNPs by Niihori *et al.*[29] However, later studies showed inhibition of the exchange reactions when membranes suitable for ligand–metal species were used to separate the reacting AuNPs.[30,31] Krishnadas *et al.* suggested an alternative mechanism wherein close contact of the nanoparticles weakens the core–monolayer interface, forming intermediate complexes with direct transfer of metal–ligand complexes between the two AuNPs.[23,32] Membrane studies by Zhang *et al.* and Su *et al.* supported this hypothesis, showing the absence of new bi-metallic species in

Department of Chemistry and Centre for Applied Materials and Related Technologies, University of Victoria, Victoria, BC, V8W 2Y2, Canada. E-mail: jdelmage@uvic.ca, ipaci@uvic.ca; Fax: +1 250-721-7147; Tel: +1 250-721-7152

ESI-MS scans.[31,33] However, further elucidation of the mechanism is limited by the inability of experimental techniques to examine directly the cluster–cluster interface during the collision process.[24,25,31]

Research efforts have turned to computational modeling to produce a mechanism for inter-cluster exchanges. Huang and Pei suggested a mechanism based on the formation of a di-anion adduct between two negatively charged clusters.[34] Using $[Au_{25}(phenylethylthiol)_{18}]^-$ and $[Ag_{25}(2,4\text{-dimethylbenzenethiol})_{18}]^-$, density functional theory calculations suggest that the first step in an inter-cluster exchange reaction is the formation of a "twist and lock" adduct structure, after which metal atom exchange through breaking and recombining the ligand shells *via* various mechanisms.[34] The formation of transient dimers has been supported by data from ESI-MS experiments and further computational modeling.[23,24]

Liu *et al.* used an *ab initio* molecular dynamics approach to study the insertion of single metal atom–thiolate adducts into $Au_{25}(SR)_{18}^-$ and $Ag_{25}(SR)_{18}^-$ nanoparticles.[35] The work proposes that ligand–metal atom adducts are inserted as a whole into the cluster, replacing pre-existing ligand–metal atom units. McCandler *et al.* used machine learned interatomic potentials to study cluster isomerization and coalescence of two $Au_{25}(SR)_{18}$ AuNPs.[36] Huang and Pei[34] used a combined method of linear synchronous transit and quadratic synchronous transit to study the energistics and potential transition states of the inter-cluster exchange mechanism between $[Au_{25}(PET)_{18}]^-$ and $[Ag_{25}(DMBT)_{18}]^-$ clusters. Their study suggests that the mechanism occurs in two distinct steps: first the exchange of a metal atom from the core of a cluster to the staple motif, followed by an exchange between staple motifs. Their mechanistic study also shows the necessary formation of a dimer structure prior to metal atom exchange.[34] Nevertheless, the dynamics of cluster collisions and the role of ligands in atom exchange have not yet been unraveled.

Here, we follow the collision of two $Au_{38-x}Ag_x(SC_2H_4Ph)_{24}$ using a direct dynamics approach. Our results suggest that the formation of dimer adducts between AuNPs occurs prior to exchange, supporting mechanisms previously proposed by others,[23,34,37] and highlighting the important role of the thiol in the exchange process. We propose a methodology for using semiempirical approaches to simulate processes in large nanostructures using direct dynamics. This method makes feasible the study of mechanisms of other transformations in nanomaterials and confined systems.

2 Models and methods

2.1 Models

We examine the process of intercluster atom transfer by following the collision of a doped $Au_{29}Ag_9(SC_2H_4Ph)_{24}$ cluster [see Fig. 1(a)–(c)] with an undoped $Au_{38}(SC_2H_4Ph)_{24}$ AuNP. These clusters take the form of a 23 atom metallic core, as shown in Fig. 1(b), surrounded by $SR(AuSC_2H_4Ph)_x$ (x = 1, 2) motifs as the monolayer [Fig. 1(c)]. Each sulfur atom is bound to a core metal

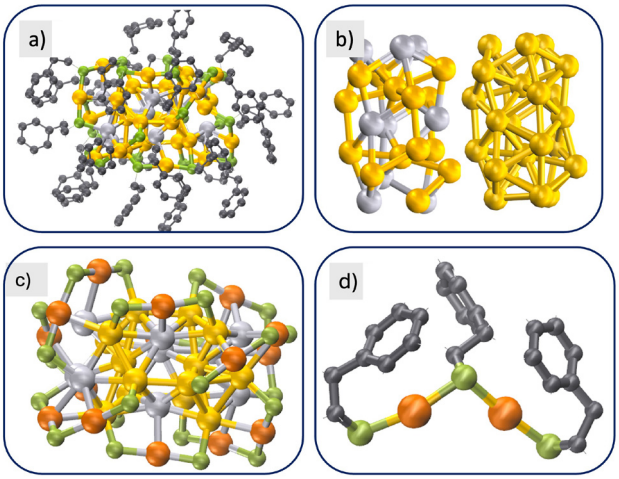

Fig. 1 Cluster models used in this work. (a) $Au_{29}Ag_9(SC_2H_4Ph)_{24}$. (b) Bi-Icosahedron cores of the $Au_{29}Ag_9$ and the Au_{38} clusters. A total of 23 atoms are in the core, including all 9 Ag atoms in the doped cluster. (c) $Au_{29}Ag_9(SC_2H_4Ph)_{24}$ with the ligands obscured for ease of viewing. Au atoms in the core are shown in yellow, while monolayer Au atoms are highlighted in orange. (d) $SC_2H_4Ph\text{-}Au\text{-}SC_2H_4Ph\text{-}Au\text{-}SC_2H_4Ph$ staple motif that forms the outer monolayer of the AuNP.

atom and a "floating" Au atom in the monolayer. These monolayer Au atoms are detached from the metal core and reside in "staple" motifs [see Fig. 1(d)], where they are each anchored by two sulfur atoms. The position of silver atoms in the core were based on X-ray crystallography data from Kumara *et al.*[38]

The entire system containing the two clusters and their ligands has 940 atoms, and running long dynamics for a system this size requires accelerated methods. As bond breaking and formation are likely key steps in the transfer process, a quantum treatment of the potential is necessary. Here, we use a "semiempirical" GFN1 method within the xTB code[39,40] for the bulk of the calculations discussed below. Unlike other semiempirical methods, such as DFTB,[41] GFN1 does not require pairwise parameters as input, instead employing both atom specific and global default parameters.

2.2 Simulating collisions – the "kick" method

We sampled collisions along a variety of trajectories. As shown in Fig. 2, the stationary cluster was centered at the origin of our unit cell. To generate different initial orientations of the colliding clusters, rotations of the stationary cluster were performed using a direction cosine matrix.[42] Further details on the sampling of the collision orientations are provided in Section S3: Details on collision trajectories.

A "kick" method was used to simulate collisions between the nanoparticles, inspired by direct dynamics, or collision dynamics methods available in the literature, and generally used for much smaller systems.[43–49] In the direct dynamics approach, initial velocities are biased to induce a collision. The reactants are followed using a non-thermalizing molecular dynamics simulation, until the collision occurs. At that point, a temperature bath is turned on if appropriate.

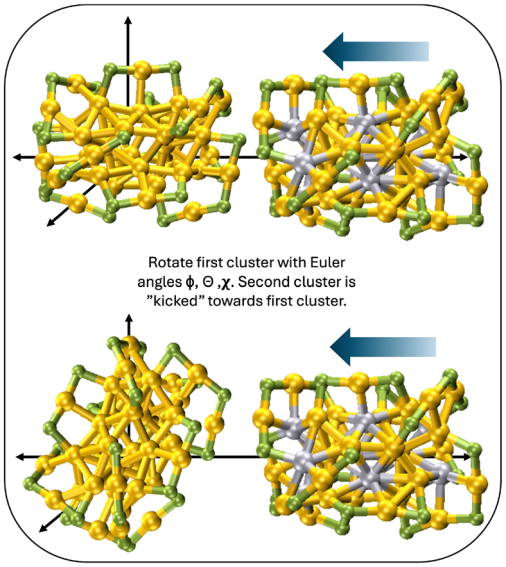

Fig. 2 Collision trajectories. The AuNP centered at the origin was rotated with a direction cosine matrix to study the effect of cluster orientation during collisions on inter-cluster exchanges.

In our method, one cluster is assigned an initial centre-of-mass ("kick") velocity while the other is initialized with zero net velocity, leading to a collision event. The time evolution of the system is then simulated using an NPT ensemble in the molecular dynamics implementation in xTB. This setup generates the same relative velocity as assigning equal and opposite velocities to both clusters. All atoms evolve freely during the simulation, and no constraints are applied. Moreover, full rethermalization after the kick takes time. To ensure that the collision takes place before the effects of the kick fully dissipate, the clusters are placed close together initially. This allows for a timely exploration of inter-cluster reactions during collisions.

The "kick" approach involves distinct steps. In the initialization step, cluster geometries are optimized individually in xTB. Also within this step, a molecular dynamics burst of 100 fs, at 300 K, provides thermalized velocities and allows the thiolate ligands to move away from their optimized structures. A 1 fs time step was used.

Step two involves manipulating velocities to invoke a collision. The mdrestart file produced by xTB at the end of the initialization process, containing atomic velocities and positions, is edited to modify the velocities of all atoms in one of the clusters. A biasing velocity, directed towards the other cluster along the intercluster axis, is added to all atom velocities. An appropriate bias must be chosen such that the clusters collide, but do not merge upon collision. This choice requires benchmarking for each system of interest.

The third step involves the simulation of the collision process, within an NPT ensemble, and starting from the altered mdrestart files. Using geometries similar to Fig. 1(a), eleven kick simulations were run for 10 ps bursts. After the initial 10 ps, trajectories that showed movement of silver atoms from the core were run for an additional 10–15 ps.

2.3 Numerical details

Simulations were performed with the xTB code using the GFN1-xTB method with a BJ-D3 dispersion treatment.[39,40,50] GFN1 was chosen over the GFN2 method due to its improved performance for inorganic clusters: GFN2 has SCC convergence issues for these systems.[51] To benchmark the accuracy of the GFN1-xTB method, we compared the average metal–sulfur bond lengths and angles for several descriptors in $Au_{29}Ag_9(SC_2H_4Ph)_{24}$ clusters optimized using GFN1 *versus* a PBE-D4/dhk-def2-SVP and a PBE-D4/def2-SVP approach in ORCA.[52–55] As shown in Fig. S1 and Table S1, the differences between the three methods for several metal–S bonds and angles were found to be within the standard deviation. For both initialization and collision simulations, we used a time step of 1 fs, and a temperature of 300 K with the default Berendsen thermostat.[56] Standard Born–Oppenheimer molecular dynamics (BOMD) initialization simulations were run for 100 fs.

Various "kick" velocities were attempted to bias the collision towards achieving exchange. Initial velocities are reduced immediately by the thermostat, as shown in Fig. S4 – as such, an oversize "kick" velocity input is required to carry out the collision. As discussed in detail in Section S2 and Fig. S4, an input velocity of 0.00025 a.u. (550 m s^{-1}) added to one cluster at the first step decays to roughly 100 m s^{-1} when ligands start moving out of the way, and to 30–50 m s^{-1} by the time the metal clusters interact. This velocity is within a standard deviation in the Maxwell–Boltzmann distribution over velocities for clusters of this size at 300 K, ensuring its physical relevance. A velocity of 40 m s^{-1} is sufficient to overcome a reaction barrier of ~0.2 eV.

3 Results and discussion

We simulate cluster collisions using pristine and silver doped $Au_{38}(SC_2H_4Ph)_{24}$. Silver exchanges between these clusters have been observed experimentally.[25,31] As the silver atoms normally reside in the core of doped AuNPs,[57] we examine first the dynamic process at the core–monolayer interface that leads to exposure of the cluster core during the collision process. Ligands are understood to have an active role in the exchange process.[33] We follow the migration of metal atoms from the core through interactions with sulfur atoms. Lastly, we discuss the implications of our direct dynamics approach and how it can be used to efficiently sample reaction timescales and mechanisms in nanomaterials.

3.1 Dynamics at the core–monolayer interface

A reactive collision event begins with a restructuring of the core–monolayer interface, the region of AuNPs where the ligands bind to the core [Fig. 1(c)]. As the two AuNPs approach each other, the phenyl groups on the thiols begin to interact

repulsively. This leads to increased dynamics at the interface, with thiols moving out of the inter-cluster region, breaking bonds between sulfur atoms and the cluster core. Once the interface breaks, metal atoms in the core are exposed and able to move into the inter-cluster region (see Fig. 3).

The figure shows the time evolution of a doped cluster in the initial stages of a collision with an AuNP. At 0 fs, the initial structure of the mixed cluster is shown. Silver atoms are buried beneath the thiolate monolayer. We follow the evolution of an Ag atom that will eventually dissociate from the doped cluster, highlighted in blue. By 9000 fs, the collision has entered its interactive regime. Thiol ligands, including the ligand bound to the highlighted atom, have begun to move out of the way, and the silver atom is approaching the cluster surface, but the sulfur–silver bond has not yet broken. The S–Ag distance indicated by the short red arrow in Fig. 3(b) has not changed significantly from the initial value of 2.5 Å. At 13 500 fs, the cluster is shown after the collision has occurred. By this point, dynamics at the core–monolayer interface has led to the breaking of the Ag–S bond, exposing the cluster core. This is reflected by the significantly larger (>4 Å) distance between the core silver atom and its previously bound thiolate.

A more detailed trajectory is shown in Fig. S8. Snapshots including both clusters throughout the collision are shown in Section S3. After the Ag–S bond is broken, the exposed Ag atom is transferred to the second cluster, with the formation of new monolayer–core bonds including the new atom.

3.2 Dependence of exchanges on collision trajectories

Multiple collision orientations were considered. Restructuring of the monolayer occurred only when the angle between the longitudinal axes of the two colliding clusters was ≤30°. End-to-end collisions were thus most likely to result in atom exchange. The surface monolayer remained intact in side-to-side or end-to-side collisions. In addition to additional ligand crowding at the sides of the cluster *versus* the ends, the surface binding modes of the ligands are also distinct. On the sides of the clusters, only monomeric staple units are present, whereas dimeric staple units are present on the ends[58,59] (see Fig. 4 for structures).

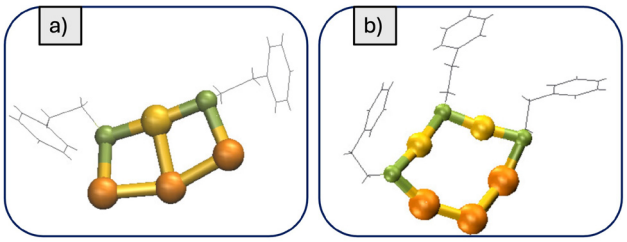

Fig. 4 Different staple units. (a) Monomeric staple unit, where both thiols are bound to the core of the cluster, found along the long sides of the clusters. (b) Dimeric staple, found at cluster ends, where the middle thiol is not bound to the core of the cluster. Core and bridging gold atoms are colored in orange and yellow, respectively, sulfurs are green.

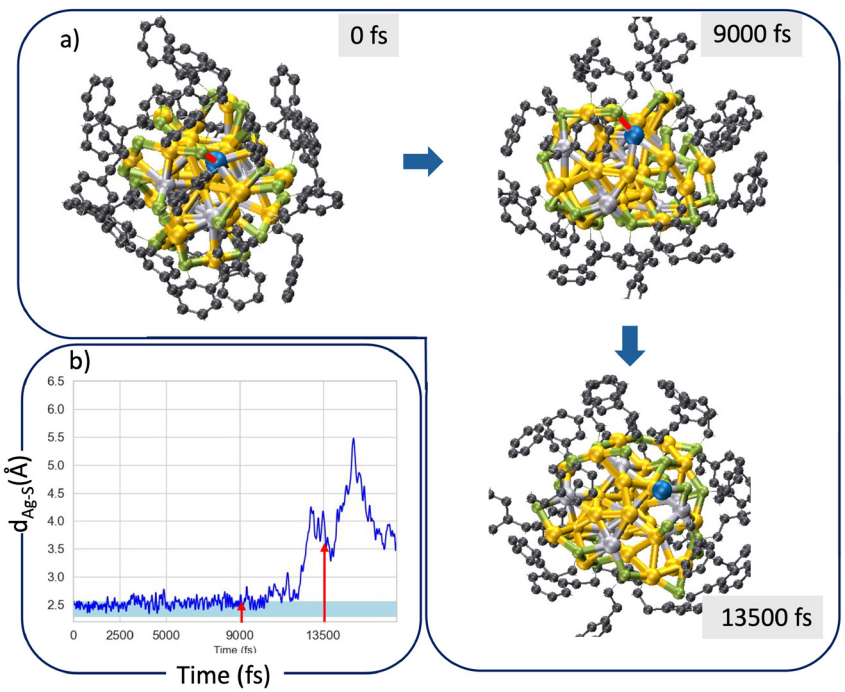

Fig. 3 Surface restructuring during the collision. The incoming cluster is shown from a viewpoint transverse to the inter-cluster axis. Panel (a) shows changes in the monolayer–core interface during the collision. The silver atom coloured in blue starts in the core and moves towards the surface. The Ag–S bond highlighted in red in the 9000 fs snapshot breaks by 13 500 fs. Panel (b) shows the distance between the silver atom and the sulfur it was initially bound to. Points on the graph highlighted with arrows correspond to the individual frames presented in (a).

In the dimeric staple units, the middle thiol is not directly bound to the core of the cluster and is more readily repositioned. This implies that the core–monolayer is more prone to restructuring around the dimeric staple units, which partly explains why exchanges occur at the end of the cluster. This is consistent with research indicating that thiols in dimeric units are more likely to participate in ligand exchange reactions.[60,61] Thus, when the clusters collide on a side-to-side trajectory, the restricted ligand movement keeps the core–monolayer interface intact and prohibits the exchange of core atoms in this region (see Fig. 5 and S9).

This is due to a combination of a more rigid monomeric staple, steric hindrance from the bulky phenyl rings, as well as π–π interactions between ligands in the two clusters preventing their folding away. In order to observe inter-cluster exchange reactions, collisions must occur on a trajectory that provides ample room for the adsorbed ligands to move and break the core–monolayer interface. This dynamic process likely depends on the specific ligand, as ligand structures are a key factor in determining cluster size, geometry and properties.[62–64] We will examine the impact of ligand identity on exchange dynamics in a future work.

3.3 Sulfur mediated exchanges

The exchange of silver atoms between AuNPs is mediated by binding to thiol groups. The formation of successive Ag–S bonds stabilizes the silver atom as it moves out of the core and undergoes the exchange process. Fig. 6 follows the silver and sulfur atoms relevant to this process throughout a simulation in which the longitudinal axes of the colliding clusters were collinear. Additional trajectories, including for other cluster orientations, are provided in Fig. S6–S10, and SI Movies end_to_end_exchange.mpg and 30_degree_rotation_exchange.mpg.

The distances between the exchanging Ag atom and the S atoms involved in the process tracked over the course of the simulation are shown in Fig. 7. Available literature indicates that Ag–S bonds are between 2.3 and 2.5 Å.[65–67] Before the collision, the exchanging Ag is positioned in the cluster core and bound to a single thiol, highlighted in red (see Fig. 6 at 0 fs). This is the unperturbed structure with a fully formed monolayer – time 0 in Fig. 7, with an Ag–S distance of ≈2.5 Å.

As clusters approach and cluster cores are exposed, the silver atom begins to migrate into the inter-cluster region. In Fig. 6, at 2250 fs the cluster cores have become exposed and Ag began to migrate from the core. This migration is accompanied by movement into the region of another thiol group from the monolayer, highlighted in green. As the silver reaches the monolayer region, it also forms a bond with a thiol (highlighted in blue) from the neighboring cluster. The blue line in Fig. 7 shows the two atoms approaching, and the bond formed at 2250 fs is maintained throughout the simulation. Roughly 300 fs later, the migrating Ag binds to a second thiol group from the target cluster, highlighted in purple, and the red-highlighted thiol moves away (see Fig. 6 and 7). The formation of these two Au–S bonds appears to help the silver enter into the inter-cluster region. The full trajectory is provided in Movie end_to_end_exhange.mpg.

Our results are consistent with the sulfur-mediated exchange mechanism proposed in DFT calculations from Huang and Pei,[34] for dianionic cluster collisions between $[Au_{25}(SR)_{18}]^-$ and $[Ag_{25}(SR)_{18}]^-$. There, formation of a highly stable dimer precedes exchange *via* several possible low-lying intermediate states (≈0.5 eV, depending on the pathway), while dimer dissociation is a slow process with a barrier of ≈2 eV. Furthermore, our work uncovers a dynamic process, where exchange is not an intrinsic consequence of cluster encounter, but arises selectively from collision geometries that allow monolayer restructuring, core exposure, and successive Ag–S interactions across the intercluster region.

Hirshfeld charges[68] for the Ag and S atoms in key frames of the trajectory presented in Fig. 6 are summarized in Table S3. Although absolute values should be interpreted with caution, the changes along the trajectory are consistent with the proposed exchange pathway. As the Ag atom leaves the core, its Hirshfeld charge becomes more positive, increasing from +0.07 at 0 fs to +0.15 at 1740 fs. At later times, charges on S_3 and S_4 become more negative than in the earlier structures, as new Ag–S contacts form at the inter-cluster region. This trend shows a redistribution of the electron density as the Ag atom moves from its original core–monolayer environment into new sulfur coordination environments. The PDOS analysis in Fig. S15 and S16 supports this interpretation by showing changes in the Ag-5s/4d and S-3p projections as exchange pro-

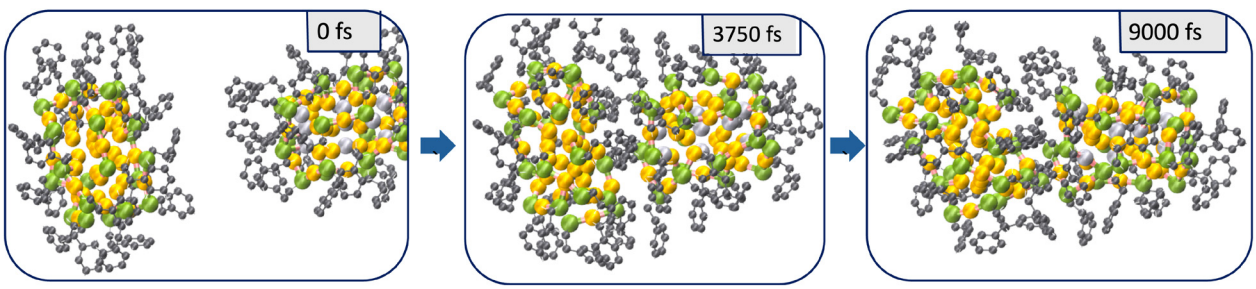

Fig. 5 Collisions without exchange. When the angle between the longitudinal axes of the two clusters was larger than ≈30° (here, 90°), ligands do not fold out of the path of the collision, preventing core exposure and metal atom exchange.

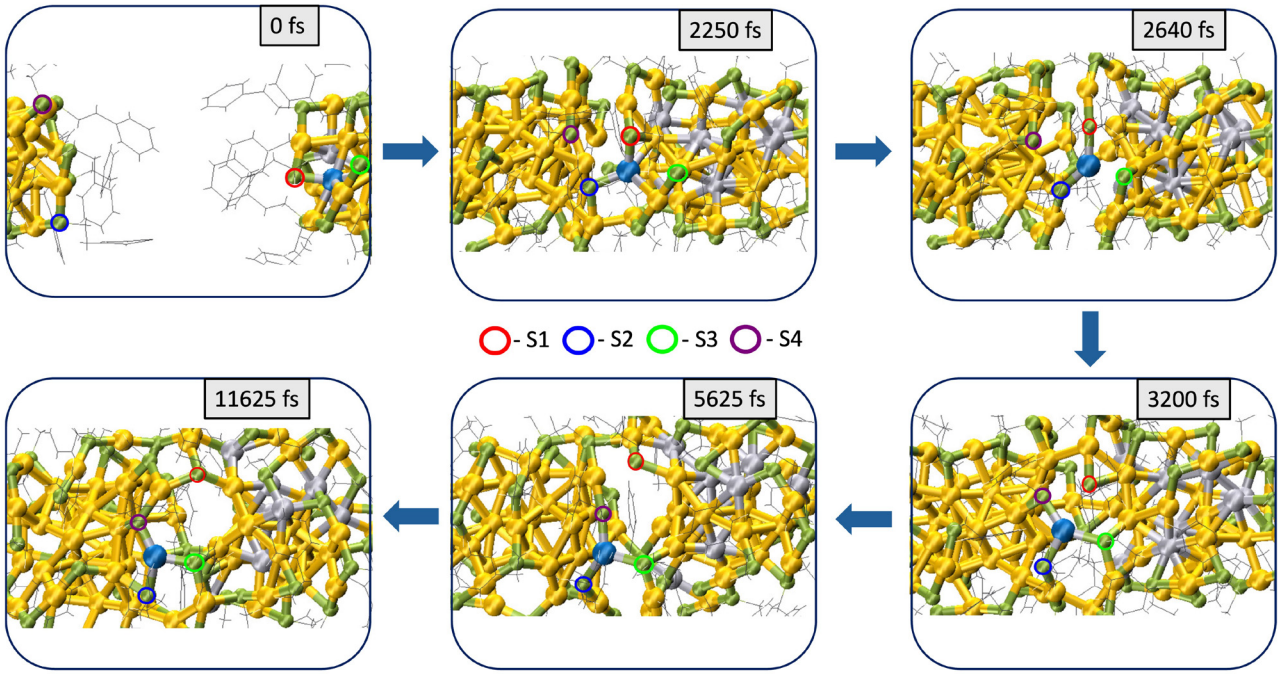

Fig. 6 Selected simulation frames showing the role of sulfur in mediating the exchange of silver atoms. Sulfur atoms are highlighted with coloured circles consistent with the plot in Fig. 7: red and green are on the incoming cluster, blue and purple on the target cluster. Corresponding simulation times are included in each snapshot.

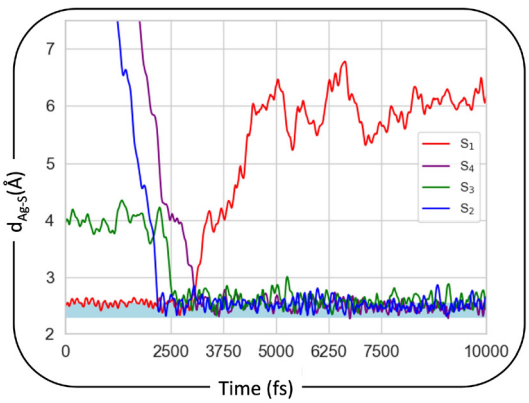

Fig. 7 Time evolution of the Ag–S distance. The distance between the silver atom highlighted in Fig. 6 and nearby sulfur atoms is shown over the initial 10 ps of a ~25 ps simulation. The literature range for Ag–S bonds is shown as light blue highlighting in the figure. S_1 is in the core–monolayer interface initially, S_3 is a nearby ligand of the mixed (incoming) cluster, whereas S_2 and S_4 are on the AuNP and bind to the Ag atom from the mixed cluster during the collision, facilitating the exchange.

ceeds. A careful examination of the frontier orbitals did not lead to any new physical insight.

No further changes were observed in the 15 000 additional time steps performed beyond 5625 fs. Relatively stable transient dimers formed at the end of the exchange simulations. Such dimers have been observed by mass spectrometry,[24,37,69] suggesting that their lifetimes may not be accessible *via* quantum simulations. Moreover, the natural formation of "magic" number clusters is likely solution- and ligand-mediated.[70,71] Simulations of the separation process have to consider a time scale several orders of magnitude longer and larger system sizes including solvent molecules, and are not computationally accessible through the methods used in this study.

We observed similar dynamics for a range of collision trajectories and cluster compositions. Exchange processes were observed for a multitude of trajectories with angles between the two clusters' longitudinal axes below 30°. Several such trajectories are shown and described in Section S3. On the other hand, trajectories in which neither cluster contained dopant atoms (collisions between pure AuNPs) indicate a different mechanism. As discussed in Section S3.5, our initial investigation of pure AuNP collisions show no reorganization of the core–monolayer interface and exchanges based only on the staple Au-SR motifs. We attribute this effect to the stronger Au–S bonding *versus* Ag–S.[72,73] However, to fully unravel these effects, systematic investigations of the dynamics of exchanges in clusters with different dopants or pure Au clusters are needed.

3.4 A direct dynamics method in a semiempirical framework

The computational approach used in this work is based on direct dynamics simulations driven by a semiempirical density-functional-based tight-binding Hamiltonian using the xTB code. The initial velocities of a pair of AuNPs are biased to incite collisions through the manipulation of restart velocities. This approach enables the simulation of an inter-cluster

exchange reaction over a computationally feasible number of time steps, while still being able to simulate bond formation and breaking.

Fig. 8 shows a trajectory comparison between two simulations with and without a biasing velocity. The top frames show similar initial geometries. Although thermalization was allowed in both cases (simulations were run in the NPT ensemble), by ≈2200 fs, the "kick" approach led to collision, whereas clusters in the BOMD simulation were still evolving separately. The final frames show the evolution of clusters after 22500 fs. In the direct dynamics simulation, we witnessed the silver atom exchange between the clusters. Again, the clusters in the BOMD simulation had not yet approached one another. In our initial explorations of this project, BOMD simulations often ultimately led to cluster approach and coalescence. However, the process was slow and a poor reflection of diffusion/collision movements in a solvent, since the kinetic energy in BOMD is randomly distributed over atomic velocities, without the collective movement leading to collisions in a solution environment. The "kick" approach provides these collective components leading to a reactive collision early in the simulation.

To the best of our knowledge, this is the first application of direct dynamics to study a pair of AuNPs. Previous applications of *ab initio*-driven direct dynamics, also known as collision dynamics, have been to simulate collisions between individual atoms, or of atoms and a surface.[43,47,49] The advent of new, high-quality semiempirical methods capable of treating transition metals and large system sizes, allow the extension of direct dynamics approaches to the study of nanoparticle collisions. In the present work, a direct-dynamics method was used to study the collision of a pair of AuNPs totaling 940 atoms.

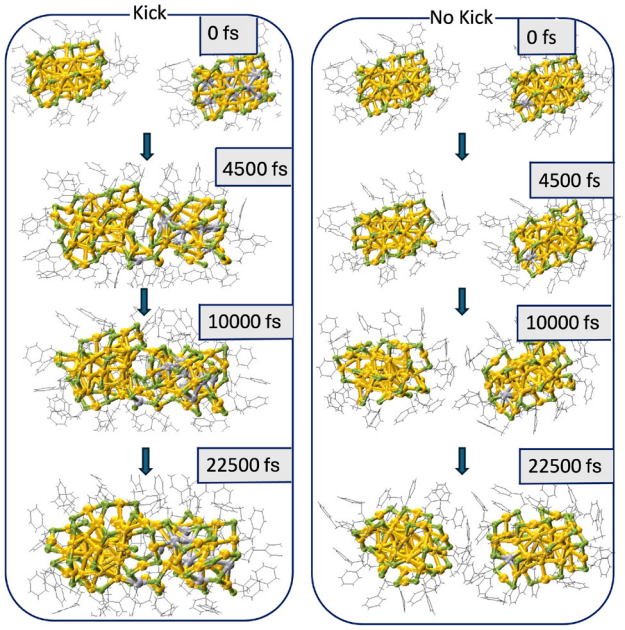

Fig. 8 Comparison of simulation trajectories with and without a kick. The trajectory in the left panel shows a reactive collision with the "kick" approach, whereas the panel on the right shows cluster evolution *via* the BOMD approach without a kick.

4 Conclusions and future work

We investigated the mechanism of inter-cluster exchange reactions between AuNPs and doped AuNPs, using a direct dynamics approach with a semiempirical level of theory. We show that the exchange mechanism is highly dependent on dynamics at the core–monolayer interface. During certain collisions, bonds at the interface break, exposing metal atoms in the cluster core. Once exposed, metal atoms from the core migrate between the clusters through interactions with thiol groups from the target cluster. The process can be followed up to the formation of metastable transient dimers, previously observed in experiments. Lastly, we discuss how modern semiempirical methods, in particular GFN1-xTB, expand our ability to study large systems using direct dynamics. This approach will allow the study of complex mechanisms in large nanomaterials, such as the nanoparticles investigated here.

Author contributions

JRRD and IP both contributed to this study's conception and design. Coding, simulations and analysis were performed by JRRD. Initial drafts of the manuscript were written by JRRD. JTP provided insight into direct dynamics simulations of intermolecular collisions and edited the manuscript. IP supervised the project, contributed to methodological design and edited the manuscript.

Conflicts of interest

There are no conflicts to declare.

Data availability

The data supporting this article have been included as part of the supplementary information (SI).

Supplementary information: optimized geometries, additional information on the "kick" method and collision trajectories, further details on exchange and non-exchange collisions examined in this work, and movie files showing different collisions. See DOI: https://doi.org/10.1039/d6nr00232c.

Acknowledgements

Funding was provided by NSERC, CFI, BCKDF and the University of Victoria. This research was performed in part using the WestGrid computing resources and the Digital Research Alliance of Canada. JRRD thanks Dr Sarah Huber of the Digital Research Alliance for software editing support.

References

1 Y. Ye and Q. Tang, *Nanoscale Horiz.*, 2025, **10**, 1597–1614.
2 S. Mussa Farkhani, P. Dehghankelishadi, A. Refaat, D. V. Gopal, A. Cifuentes-Rius and N. H. Voelcker, *Prog. Mater. Sci.*, 2024, **142**, 101229.
3 R. Jin, *Nanoscale*, 2010, **2**, 343–362.
4 I. Chakraborty and T. Pradeep, *Chem. Rev.*, 2017, **117**, 8208–8271.
5 H. Qian, W. T. Eckenhoff, Y. Zhu, T. Pintauer and R. Jin, *J. Am. Chem. Soc.*, 2010, **132**, 8280–8281.
6 M. M. Mariscal, J. A. Olmos-Asar, C. Gutierrez-Wing, A. Mayoral and M. J. Yacaman, *Phys. Chem. Chem. Phys.*, 2010, **12**, 11785–11790.
7 M. Rambukwella, S. Burrage, M. Neubrander, O. Baseggio, E. Aprà, M. Stener, A. Fortunelli and A. Dass, *J. Phys. Chem. Lett.*, 2017, **8**, 1530–1537.
8 J. B. Tracy, M. C. Crowe, J. F. Parker, O. Hampe, C. A. Fields-Zinna, A. Dass and R. W. Murray, *J. Am. Chem. Soc.*, 2007, **129**, 16209–16215.
9 N. Yan, N. Xia, L. Liao, M. Zhu, F. Jin, R. Jin and Z. Wu, *Sci. Adv.*, 2018, **4**, eaat7259.
10 M. Dasog, W. Hou and R. W. J. Scott, *Chem. Commun.*, 2011, **47**, 8569–8571.
11 C.-k. Kim, P. Ghosh and V. M. Rotello, *Nanoscale*, 2009, **1**, 61–67.
12 J. M. Abad, M. Pita and A. L. De Lacey, *J. Phys. Chem. Lett.*, 2023, **14**, 1452–1456.
13 Y. Zhu, H. Qian, M. Zhu and R. Jin, *Adv. Mater.*, 2010, **22**, 1915–1920.
14 J. Gao, X. Huang, H. Liu, F. Zan and J. Ren, *Langmuir*, 2012, **28**, 4464–4471.
15 S. Knoppe, M. Vanbel, S. van Cleuvenbergen, L. Vanpraet, T. Bürgi and T. Verbiest, *J. Phys. Chem. C*, 2015, **119**, 6221–6226.
16 T. Ishida, T. Murayama, A. Taketoshi and M. Haruta, *Chem. Rev.*, 2020, **120**, 464–525.
17 S. Wang, X. Meng, A. Das, T. Li, Y. Song, T. Cao, X. Zhu, M. Zhu and R. Jin, *Angew. Chem., Int. Ed.*, 2014, **53**, 2376–2380.
18 C. Garcia, V. Truttmann, I. Lopez, T. Haunold, C. Marini, C. Rameshan, E. Pittenauer, P. Kregsamer, K. Dobrezberger, M. Stöger-Pollach, N. Barrabés and G. Rupprechter, *J. Phys. Chem. C*, 2020, **124**, 23626–23636.
19 Y. Negishi, K. Igarashi, K. Munakata, W. Ohgake and K. Nobusada, *Chem. Commun.*, 2011, **48**, 660–662.
20 T. Cesca, B. Kalinic, N. Michieli, C. Maurizio, A. Trapananti, C. Scian, G. Battaglin, P. Mazzoldi and G. Mattei, *Phys. Chem. Chem. Phys.*, 2015, **17**, 28262–28269.
21 R. Jin and K. Nobusada, *Nano Res.*, 2014, **7**, 285–300.
22 H. Qian, D.-e. Jiang, G. Li, C. Gayathri, A. Das, R. R. Gil and R. Jin, *J. Am. Chem. Soc.*, 2012, **134**, 16159–16162.
23 K. R. Krishnadas, A. Baksi, A. Ghosh, G. Natarajan, A. Som and T. Pradeep, *Acc. Chem. Res.*, 2017, **50**, 1988–1996.
24 M. Neumaier, A. Baksi, P. Weis, E. K. Schneider, P. Chakraborty, H. Hahn, T. Pradeep and M. M. Kappes, *J. Am. Chem. Soc.*, 2021, **143**, 6969–6980.
25 B. Zhang and T. Bürgi, *J. Phys. Chem. C*, 2016, **120**, 4660–4666.
26 N. Müller, R. Banu, A. Loxha, F. Schrenk, L. Lindenthal, C. Rameshan, E. Pittenauer, J. Llorca, J. Timoshenko, C. Marini and N. Barrabés, *Commun. Chem.*, 2023, **6**, 1–10.
27 S. Hossain, D. Suzuki, T. Iwasa, R. Kaneko, T. Suzuki, S. Miyajima, Y. Iwamatsu, S. Pollitt, T. Kawawaki, N. Barrabés, G. Rupprechter and Y. Negishi, *J. Phys. Chem. C*, 2020, **124**, 22304–22313.
28 Y. Song, T. Huang and R. W. Murray, *J. Am. Chem. Soc.*, 2003, **125**, 11694–11701.
29 Y. Niihori, W. Kurashige, M. Matsuzaki and Y. Negishi, *Nanoscale*, 2013, **5**, 508–512.
30 G. Salassa, A. Sels, F. Mancin and T. Bürgi, *ACS Nano*, 2017, **11**, 12609–12614.
31 B. Zhang, G. Salassa and T. Bürgi, *Chem. Commun.*, 2016, **52**, 9205–9207.
32 K. R. Krishnadas, A. Ghosh, A. Baksi, I. Chakraborty, G. Natarajan and T. Pradeep, *J. Am. Chem. Soc.*, 2016, **138**, 140–148.
33 H.-F. Su, H. Deng, L.-S. Zheng and B. K. Teo, *Inorg. Chem.*, 2025, **64**, 10478–10487.
34 B. Huang and Y. Pei, *J. Mater. Chem. A*, 2020, **8**, 10242–10251.
35 H. Liu, B. Huang, Y. Shao and Y. Pei, *Small*, 2024, **20**, 2403520.
36 C. A. McCandler, A. Pihlajamäki, S. Malola, H. Häkkinen and K. A. Persson, *ACS Nano*, 2024, **18**, 19014–19023.
37 A. Baksi, P. Chakraborty, S. Bhat, G. Natarajan and T. Pradeep, *Chem. Commun.*, 2016, **52**, 8397–8400.
38 C. Kumara, C. M. Aikens and A. Dass, *J. Phys. Chem. Lett.*, 2014, **5**, 461–466.
39 C. Bannwarth, E. Caldeweyher, S. Ehlert, A. Hansen, P. Pracht, J. Seibert, S. Spicher and S. Grimme, *Wiley Interdiscip. Rev.: Comput. Mol. Sci.*, 2021, **11**, e1493.
40 S. Grimme, C. Bannwarth and P. Shushkov, *J. Chem. Theory Comput.*, 2017, **13**, 1989–2009.
41 B. Hourahine, B. Aradi, V. Blum, F. Bonafé, A. Buccheri, C. Camacho, C. Cevallos, M. Deshaye, T. Dumitrică, A. Dominguez, S. Ehlert, M. Elstner, T. van der Heide, J. Hermann, S. Irle, J. J. Kranz, C. Köhler, T. Kowalczyk, T. Kubař, I. S. Lee, V. Lutsker, R. J. Maurer, S. K. Min, I. Mitchell, C. Negre, T. A. Niehaus, A. M. N. Niklasson, A. J. Page, A. Pecchia, G. Penazzi, M. P. Persson, J. Řezáč, C. G. Sánchez, M. Sternberg, M. Stöhr, F. Stuckenberg, A. Tkatchenko, V. W.-z. Yu and T. Frauenheim, *J. Chem. Phys.*, 2020, **152**, 124101.
42 R. N. Zare, *Angular momentum : understanding spatial aspects in chemistry and physics*, Wiley, New York, 1988.
43 J. T. Paci and I. Paci, *J. Phys. Chem. C*, 2019, **123**, 29647–29655.
44 L. Y. Yeung, M. Okumura, J. Zhang, T. K. Minton, J. T. Paci, A. Karton, J. M. L. Martin, J. P. Camden and G. C. Schatz, *J. Phys. Chem. A*, 2012, **116**, 64–84.
45 L. Zhan, H. Chen, H. Zhou, J. Chen, H. Wu and L. Yang, *Powder Technol.*, 2023, **422**, 118456.
46 A. Malik, L. A. Angel, R. Spezia and W. L. Hase, *Phys. Chem. Chem. Phys.*, 2020, **22**, 14551–14559.

47 K. Bolton and A. Rosén, *Phys. Chem. Chem. Phys.*, 2002, **4**, 4481–4488.
48 S. Lakshmanan, H. Kim and W. L. Hase, *RSC Adv.*, 2021, **11**, 16173–16178.
49 B. Jayee, R. Nieman, T. K. Minton, W. L. Hase and H. Guo, *J. Phys. Chem. C*, 2021, **125**, 9795–9808.
50 S. Grimme, J. Antony, S. Ehrlich and H. Krieg, *J. Chem. Phys.*, 2010, **132**, 154104.
51 C. Bannwarth, S. Ehlert and S. Grimme, *J. Chem. Theory Comput.*, 2019, **15**, 1652–1671.
52 F. Neese, F. Wennmohs, U. Becker and C. Riplinger, *J. Chem. Phys.*, 2020, **152**, 224108.
53 J. P. Perdew, K. Burke and M. Ernzerhof, *Phys. Rev. Lett.*, 1996, **77**, 3865–3868.
54 F. Weigend and R. Ahlrichs, *Phys. Chem. Chem. Phys.*, 2005, **7**, 3297–3305.
55 B. A. Hess, *Phys. Rev. A*, 1986, **33**, 3742–3748.
56 H. J. C. Berendsen, J. P. M. Postma, W. F. van Gunsteren, A. DiNola and J. R. Haak, *J. Chem. Phys.*, 1984, **81**, 3684–3690.
57 C. Kumara, K. J. Gagnon and A. Dass, *J. Phys. Chem. Lett.*, 2015, **6**, 1223–1228.
58 H. Qian, W. T. Eckenhoff, Y. Zhu, T. Pintauer and R. Jin, *J. Am. Chem. Soc.*, 2010, **132**, 8280–8281.
59 S. Pollitt, V. Truttmann, T. Haunold, C. Garcia, W. Olszewski, J. Llorca, N. Barrabés and G. Rupprechter, *ACS Catal.*, 2020, **10**, 6144–6148.
60 B. Molina, A. Sánchez-Castillo, S. Knoppe, I. L. Garzón, T. Bürgi and A. Tlahuice-Flores, *Nanoscale*, 2013, **5**, 10956–10962.
61 A. Fernando and C. M. Aikens, *J. Phys. Chem. C*, 2016, **120**, 14948–14961.
62 Y. Wang and T. Bürgi, *Nanoscale Adv.*, 2021, **3**, 2710–2727.
63 Y. Su, Y. Xie and R. Jin, *Inorg. Chem.*, 2026, **65**, 428–440.
64 R. Jin, *Nanoscale*, 2010, **2**, 343–362.
65 S. I. Sadovnikov, M. G. Kostenko, A. I. Gusev and A. V. Lukoyanov, *Nanomaterials*, 2023, **13**, 2638.
66 Z. Tian, C. Song and C. Wang, *J. Nanopart. Res.*, 2022, **24**, 104.
67 Q. Wang, S.-L. Dong, D.-D. Tao, Z. Li and Y.-B. Jiang, *Coord. Chem. Rev.*, 2021, **432**, 213717.
68 F. L. Hirshfeld, *Theor. Chim. Acta*, 1977, **44**, 129–138.
69 X. Liu, G. Saranya, X. Huang, X. Cheng, R. Wang, M. Chen, C. Zhang, T. Li and Y. Zhu, *Angew. Chem., Int. Ed.*, 2020, **59**, 13941–13946.
70 O. Toikkanen, S. Carlsson, A. Dass, G. Rönnholm, N. Kalkkinen and B. M. Quinn, *J. Phys. Chem. Lett.*, 2009, **1**, 32–37.
71 R. Kazan, U. Müller and T. Bürgi, *Nanoscale*, 2019, **11**, 2938–2945.
72 S. Kim, K. Ihm, T. Kang, S. Hwang and S. Joo, *Surf. Interface Anal.*, 2005, **37**, 294–299.
73 K. A. Kacprzak, O. Lopez-Acevedo, H. Häkkinen and H. Grönbeck, *J. Phys. Chem. C*, 2010, **114**, 13571–13576.